Technical Note

Subduction and Shallow Earthquake Demand on Coupled Composite Plate Shear Wall–Concrete-Filled System

Ashim Koirala[1]; Emre Kizilarslan, S.M.ASCE[2]; Michel Bruneau, Dist.M.ASCE[3]; and Robert Tremblay[4]

Abstract: This brief technical note compares the adjusted collapsed margin ratios for concrete-filled coupled composite plate steel walls, as obtained from the FEMA P695 methodology, separately considering only subduction zone earthquakes and only shallow earthquakes. For shallow earthquakes, collapse margin ratios were similar to those obtained in prior studies, but they were substantially smaller for the set of subduction earthquakes. While both sets of collapse margin ratios were considered to provide satisfactory seismic performance, this study provides insights into the impact of considering subduction earthquakes in FEMA P695 studies and, by inference, on expected collapse margin ratio for subduction earthquakes. **DOI: 10.1061/JSENDH.STENG-12704.**

Author keywords: Coupled composite plate shear walls; Seismic performance; Collapse; Seismic performance factors; FEMA P695 methodology; Seismic effects; Subduction earthquakes.

Introduction

The coupled composite plate shear wall–concrete filled (CC-PSW/CF) system is a structural system for which seismic design provisions have been recently included in design specifications (AISC 2022b), on the strength of much research (Kizilarslan et al. 2021a, b; Bruneau et al. 2019, 2021; Kizilarslan and Bruneau 2023; Kenarangi et al. 2020; Broberg et al. 2022; Shafaei et al. 2021). Multiple articles on the recently completed 850-ft- (259-m-) tall 58-story Rainier Square Tower in Seattle and the 200 Park building in San Jose (AISC 2021) have documented the advantages of this structural system in accelerating construction time (AISC 2019). At the time of this writing, other projects are in the planning stage.

In the research that led to the seismic design provisions for CC-PSW/CF added to ASCE 7-22 and to AISC-341-22, the FEMA P695 methodology (FEMA 2009) was used to validate proposed seismic design parameters—namely, a response modification factor (R) of 8, an overstrength factor (Ω_0) of 2.5, and a deflection amplification factor (C_d) of 5.5 (Kizilarslan et al. 2021a). In essence, the FEMA P695 procedure relies on incremental dynamic analysis (IDA) to determine the collapse strength of various archetypes designed per the proposed procedure, and compare that collapse strength against the strength at the maximum considered earthquake (MCE) design level, thus establishing a corresponding adjusted collapse margin ratio (ACMR)—"adjusted" because it is also multiplied by adjustment factors. For a structural system to be deemed to have satisfactory seismic performance, this margin against collapse must exceed values prescribed by FEMA P695. More specifically, the ACMR of individual archetypes and the average ACMR of a group of archetypes should be greater than the 20% ($\mathrm{ACMR}_{20\%}$) and 10% ($\mathrm{ACMR}_{10\%}$) collapse probability under MCE, respectively. Total system collapse uncertainty (β_{TOT}) is needed in order to calculate the acceptable ACMR value. The value of β_{TOT} is obtained by combining uncertainty factors related to record-to-record (β_{RTR}), design requirements (β_{DR}), test data (β_{TD}), and nonlinear modeling (β_{MDL}) using Eq. (1). For the selected ground motions used in the FEMA P695 methodology, a constant value of β_{RTR} equal to 0.4 is used, given that period-based ductility is greater than or equal to 3 ($\mu_T \geq 3$). The other three uncertainty factors (β_{DR}, β_{TD}, and β_{MDL}) were taken as equal to 0.2, corresponding to the "good" rating (i.e., β_{DR}, β_{TD}, and $\beta_{\mathrm{MDL}} = 0.2$). The corresponding total system uncertainty calculated using Eq. (1) is 0.529. The acceptable ACMR for 10% and 20% collapse probability under MCE ground motions (i.e., $\mathrm{ACMR}_{10\%}$ and $\mathrm{ACMR}_{20\%}$) for β_{TOT} of 0.529 is specified to be 1.96 and 1.56 in Tables 9–7 of the FEMA P695 document, respectively

$$\beta_{\mathrm{TOT}} = \sqrt{\beta_{\mathrm{RTR}}^2 + \beta_{DR}^2 + \beta_{TD}^2 + \beta_{\mathrm{MDL}}^2} \tag{1}$$

To meet the interest of engineers in using CC-PSW/CF in Canada, there was a need to repeat part of the previous FEMA P695 studies for a set of ground motions deemed more representative of Canadian applications. This was particularly driven by the fact that the suite of ground motions being considered in the development of a Canadian methodology similar to FEMA P695 included a series of subduction zone earthquakes (Fazileh et al. 2023). This provided an opportunity to investigate the impact of subduction zone earthquakes on CC-SPW/CF, which is of interest in many parts of the world, including the US Pacific Northwest. Thus, this technical note presents the results of FEMA P695 analyses conducted independently considering a set of shallow crustal earthquakes and a set of subduction earthquakes to assess the impact of the more severe set on the ACMR of CC-PSW/CF. This provides insight into the respective impact of each type of earthquake and will be helpful for future reference.

[1]Research Assistant, Dept. of Civil, Structural and Environmental Engineering, Univ. at Buffalo, Buffalo, NY 14260. ORCID: https://orcid.org/0009-0008-0171-3236. Email: ashimkoi@buffalo.edu

[2]Structural Engineer, Thornton Tomasetti, 707 Wilshire Blvd., Suite 4450, Los Angeles, CA 90017 (corresponding author). ORCID: https://orcid.org/0000-0003-3014-1165. Email: emrekizi@buffalo.edu

[3]SUNY Distinguished Professor, Dept. of Civil, Structural and Environmental Engineering, Univ. at Buffalo, Buffalo, NY 14260. ORCID: https://orcid.org/0000-0003-1170-468X. Email: bruneau@buffalo.edu

[4]Professor, Dept. of Civil Engineering, Ecole Polytechnique, Montreal, QC, Canada. Email: robert.tremblay@polymtl.ca

Note. This manuscript was submitted on April 18, 2023; approved on February 28, 2024; published online on June 3, 2024. Discussion period open until November 3, 2024; separate discussions must be submitted for individual papers. This technical note is part of the ***Journal of Structural Engineering***, © ASCE, ISSN 0733-9445.

Table 1. Suite of 12 records from shallow crustal earthquakes

Station No.	NGA-West2 RSN	Event date and name	Magnitude	Station	VS30 (m/s)	R_{rup} (km)	Comp
1	4,866	2007 Chuetsu-oki	6.8	Kawanishi Izumozaki	338	12	EW
2	960	1994 Northridge	6.69	Canyon Country–W Lost Cany	326	12	270°
3	1,082	1994 Northridge	6.69	Sun Valley–Roscoe Blvd	321	10	0°
4	1,003	1994 Northridge	6.8	LA–Saturn St	309	27	110°
5	4,886	2007 Chuetsu-oki	6.69	Tamati Yone Izumozaki	338	11	NS
6	313	1981 Corinth	6.8	Corinth	361	10	T
7	995	1994 Northridge	6.6	LA–Hollywood Stor FF	316	24	360°
8	725	1987 Superstition Hills-02	6.69	Poe Road (temp)	317	11	360°
9	987	1994 Northridge	6.54	LA–Centinela St	322	28	245°
10	1,042	1994 Northridge	6.69	N. Hollywood–Coldwater Can	326	12	270°
11	3,749	1992 Cape Mendocino	7.01	Fortuna Fire Station	355	20	360°
12	953	1994 Northridge	6.69	BeverlyHills–14145 Mulhol	356	17	279°
		Average value	6.7		332	16	

Note: RSN = record sequence number; R_{rup} = rupture distance; Comp = component; EW = east-west; and NS = north-south. 1 m/s = 2.24 mi/h and 1 km = 0.62 mi.

Table 2. Suite of 8 records from shallow in-slab earthquakes

Station No.	No.	Event date and name	Magnitude	Station	Site cl	R_{hyp}	Comp
1	N001001	2001 El Salvador	7.7	San Pedro Nonualco	D	91	0°
2	EHM003	2001 Geiyo	6.8	Tohyo	D	63	EW
3	1416a	2001 Nisqually	6.8	West Seattle, Fire Station 29	D	76	125°
4	EHM015	2001 Geiyo	6.8	Nagahama	D	77	EW
5	4355a	2001 El Salvador	7.7	Santiago de Maria	C/D	95	90°
6	HRS014	2001 Geiyo	6.8	Ohno	D	63	NS
7	Za01003	2001 El Salvador	7.7	Zacatecoluca	C/D	84	360°
8	HRS0190	2001 Geiyo	6.8	Kure	D	50	EW
		Average value	7.1			73	

Note: Site cl = site class; R_{hyp} = closest distance to the rupture plane; Comp = component; EW = east-west; and NS = north-south.

Table 3. Suite of 20 records from subduction interface earthquakes

Station No.	Event date and name	Magnitude	Station name	Site cl	R_{cd} (km)	Comp
1	2003 Tokachi-oki	8.3	Monbetsu-W	D	106	EW
2	2003 Tokachi-oki	8.3	Monbetsu	C	104	EW
3	2003 Tokachi-oki	8.3	Biratori-W	C	106	NS
4	2011 Tohoku	9.1	Towadako-E	D	145	NS
5	2011 Tohoku	9.1	Iwaki-E	D	112	NS
6	2011 Tohoku	9.1	Hasunuma	D	164	NS
7	2003 Tokachi-oki	8.3	Biratori	D	104	NS
8	2011 Tohoku	9.1	Shimodate	C	161	NS
9	2003 Tokachi-oki	9.1	Kuriyama	D	151	NS
10	2011 Tohoku	9.1	Towada	D	143	NS
11	2011 Tohoku	9.1	Nakoso	D	119	EW
12	2011 Tohoku	9.1	Yaita	D	162	NS
13	2011 Tohoku	9.1	Onoda	D	125	EW
14	2011 Tohoku	9.1	Iwanuma	D	115	NS
15	2011 Tohoku	9.1	Kanegasaki	C	120	NS
16	2011 Tohoku	9.1	Naruko	D	137	EW
17	2011 Tohoku	9.1	Hisaki-2	D	145	EW
18	2011 Tohoku	9.1	Yaita	C	168	NS
19	2011 Tohoku	9.1	Yohkaichiba	D	156	NS
20	2003 Tokachi-oki	8.3	Shihoro	D	98	NS
	Average value	8.9			132	

Note: Site cl = site class; R_{cd} = closest distance from fault plane; Comp = component; EW = east-west; and NS = north-south. 1 km = 0.62 mi.

Ground Motions

In the study presented here, two suites of 20 ground motion records were considered for the analysis of archetypes. These consisted of one suite of 20 records from shallow crustal earthquakes (Table 1) and in-slab earthquakes (Table 2) and another suite of 20 records from interface subduction earthquakes (Table 3). The selection of ground motions was performed in accordance with the procedure specified in the National Building Code of Canada. The resulting comparison with design spectra showed adequate scatter to prevent

Table 4. Three-story archetypes

Case	No. of stories	Coupled wall length (in.)	Wall thickness, t_{sc} (in.)	Plate thickness, t_p (in.)	CB length (in.)	CB section (in.)	Design CR (%)	Performance group
1	3	120	12	1/8	120	12 × 24 × 1/2(f), 3/8(w)	63.1	5
2	3	120	12	3/16	120	12 × 24, 3/8(f), 3/8(w)	47.6	15

Note: CB = coupling beam; and CR = coupling ratio. 1 in. = 25.4 mm.

Table 5. Eight-story archetypes

Case	No. of Stories	L/d	Cs	Coupled wall length (in.)	Wall thickness, t_{sc} (in.)	Plate thickness, t_p (in.)	CB length (in.)	CB section (in.)	Uncoupled wall length (in.)	Performance group
PG-1A	8	3	0.076	144	20	9/16	72	20 × 24 × 3/8(f), 3/8(w)	252	1
PG-1C	8	5	0.076	120	24	5/8	120	24 × 24 × 1/2(f), 3/8(w)	240	1

Note: L = length of coupling beam; d = depth of coupling beam; Cs = equivalent lateral load factor; and CB = coupling beam. 1 in. = 25.4 mm.

Table 6. Eighteen-story archetypes

Case	No. of stories	L/d	Cs	C wall depth (in.; c-c)	C wall width (in.; c-e)	$t_{sc.f}$ (in.)	$t_{sc.w}$ (in.)	$t_{p.\mathrm{bot}}$ (in.)	$t_{p.\mathrm{top}}$ (in.)	CB length (in.)	CB section (in.)	Performance group
PG-3A	18	3	0.042	360	180	18	14	1/2	5/16	72	18 × 24 × 5/16 (f), 3/8 (w)	3
PG-3C	18	5	0.042	360	156	26	16	9/16	5/16	120	26 × 24 × ½ (f), 3/8 (w)	3

Note: L = length of coupling beam; d = depth of coupling beam; Cs = equivalent lateral load factor; and CB = coupling beam. 1 in. = 25.4 mm.

bias in the study results. Also, Bebamzadeh et al. (2023) showed that seismic hazard disaggregation for long period structures in Vancouver for a probability of exceedance of 2% in 50 years is driven by M > 8.3 earthquakes, with a median of M 8.8. For the Cascadia subduction zone, only records from the Tohoku and Tokachi-oki earthquakes met this criterion with sufficient Arias intensity and duration to be deemed representative of this region.

Six of the archetypes described by Kizilarslan et al. (2021a) were selected for the analyses: selecting, from each of the 3-story, 8-story, and 18-story archetypes, the one that Kizilarslan et al. (2021a) reported as having the lowest collapse margin ratio, and the one with highest collapse margin ratio for the group. These were designed for an $R = 8$ value. Modeling of the archetypes was also identical to Kizilarslan et al. in all aspects. Likewise, as CC-PSW/CF wall collapse typically happened at drifts much greater than 5%, the point at which a 5% drift was reached was defined as corresponding to "collapse" for the purpose of the IDA analyses (unless, evidently, collapse actually occurred at a lower drift value), as in prior FEMA P695 CC-PSW/CF studies.

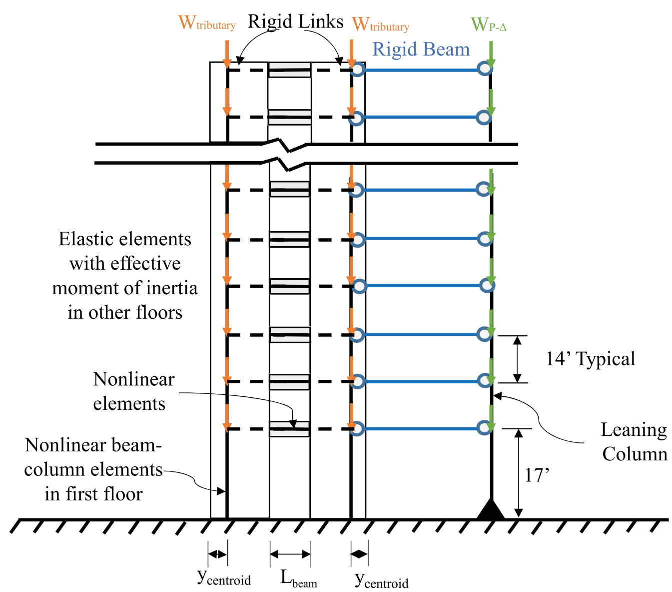

Fig. 1. Nonlinear model for simulating collapse of coupled C-PSW/CF wall system ($y_{\mathrm{centroid}} = d_{\mathrm{wall}}/2$ for planar walls).

Archetypes

The CC-PSW/CF archetypes used in this study consisted of uncoupled planar walls (Type I) for lower-rise buildings, coupled C-shaped walls (Type II) for higher-rise buildings. The coupling beams were composite box cross sections. The maximum considered seismic demand for this system was Design Category D. Only the maximum seismic design parameters ($D_{\max}$ for which design spectral accelerations are $S_{DS} = 1.0$ g and $S_{D1} = 0.6$ g) were evaluated per the FEMA P695 procedure. The height of the structure influenced both the period and the wall configuration of the archetypes. Properties of the archetypes selected for the FEMA P695 study are listed in Tables 4–6.

Fig. 1 shows the two-dimensional (2D) nonlinear model used for the collapse simulation of CC PSW/CF archetypes. *ReinforcingSteel* (McKenna et al. 2016) and *Concrete02* material models in the OpenSees library (McKenna et al. 2016) were used for steel and concrete fibers in the cross sections of planar and C-shaped walls. Note that the steel inelastic hysteretic model used in the fiber analyses was selected because of its ability to track cyclic strain demands and remove fibers when their low-cycle fatigue life is reached, which is the most important way in which strength degradation takes place in this type of composite wall, as was observed experimentally by Kenarangi et al. (2020) and Kizilarslan and Bruneau (2023), and verified analytically by Kizilarslan et al. (2021b). Details can be found in Kizilarslan et al. (2021a). For walls, the nonlinear beam-column elements were assigned only to the first floor and the rest of the floors were modeled using elastic beam-column elements having effective stiffness per Eq. (I2-12) in AISC 341-22 (AISC 2022a), whereas the coupling beams were modeled using only nonlinear beam-column elements. Leaning columns of insignificant flexural stiffness were added to the structural model to capture the P-Δ effects in given stories due to gravity loads that were not located on the CC-PSW/CF system itself [1,440 kips (6,405 kN)]. Tributary loads coming to

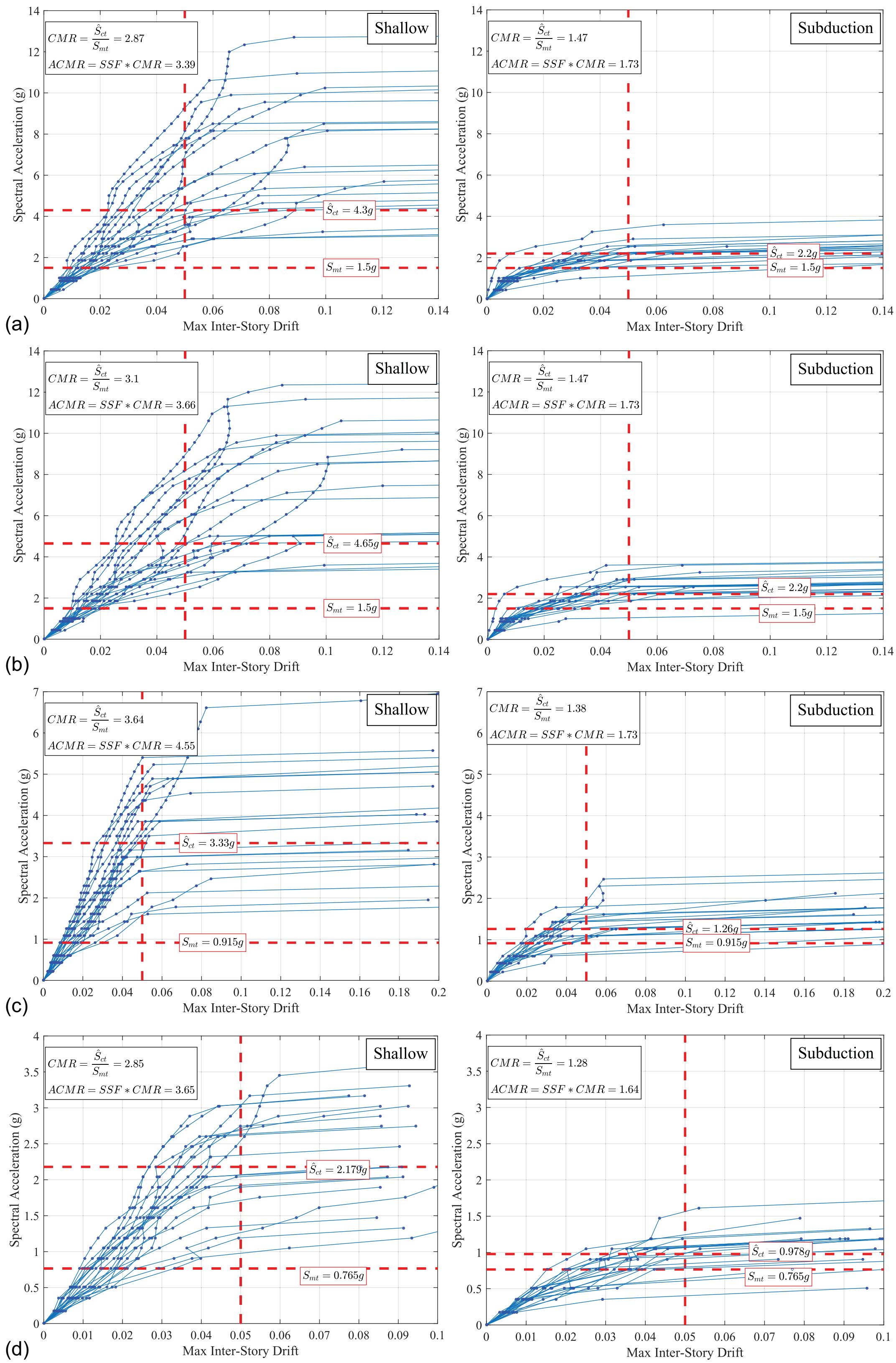

Fig. 2. IDA for shallow and subduction zone earthquakes: (a) PG-ThreeStory; (b) PG-ThreeStory2; (c) PG-1A; (d) PG-1C; (e) PG-3A; and (f) PG-3C.

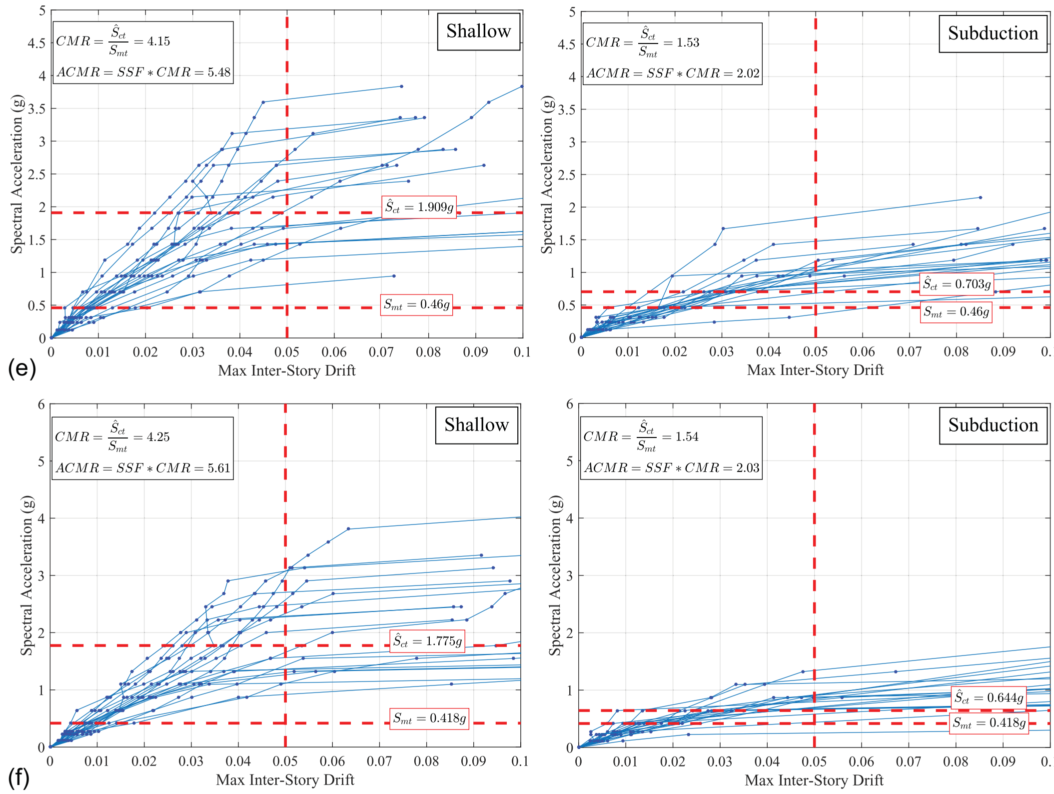

Fig. 2. (*Continued.*)

the C-PSW/CF walls [72 kips (320 kN) per floor for planar walls; 144 kips (640 kN) for C-Shaped walls] were applied to the wall in each floor. Rigid links were assigned between the C-PSW/CF wall center of gravity and the point where the coupling beams frame into the walls, and rigid beams were used to connect the leaning column and the C-PSW/CF wall at every floor. No seismic mass was assigned to the leaning column; seismic masses were applied to the C-PSW/CF walls and distributed equally to the column's left and right joints at every story. The damping ratio was calculated based on the height of the structure, in accordance with the following equation from PEER Section 4.2.7 (PEER 2017):

$$\xi_{\text{critical}} = \frac{0.36}{\sqrt{H}} \tag{2}$$

where H is the height of the structure in feet.

After further study of the behavior of these lateral load resisting systems, it was observed that the composite walls were vibrating individually at a much larger period of vibration after buckling or fracture developed, and that the response eventually transformed into a rocking behavior after excessive damage in the plastic hinge region. As a result, the period of the system elongated significantly as it progressed toward that stage of severe damage. In order to prevent overdamping of the structural system when it shifted to those higher periods of vibration (Kizilarslan et al. 2021a), it was decided to perform these analyses with a reduced damping ratio anchored at five times the first period and at the fourth period of vibration of the walls.

Results for Different Earthquake Types

Results from the FEMA P695 study are presented in Fig. 2, as well as in Tables 7 and 8 for shallow earthquakes and subduction earthquakes, respectively. For shallow earthquakes, the resulting ACMRS were on the same orders of magnitude as those obtained by Kizilarslan et al. (2021a), even though the set of earthquakes

Table 7. IDA results for shallow earthquakes only

Group	Archetype	$\hat{S}_{CT}$ (g)	S_{MT} (g)	CMR	SSF	ACMR	Pass/fail	ACMR_{ave}	Pass/fail
3-story	PG-ThreeStory	4.30	1.50	2.87	1.18	3.39	Pass	3.52	Pass
	PG-ThreeStory2	4.65	1.50	3.10	1.18	3.66	Pass		
8-story	PG-1A	3.25	0.92	3.64	1.25	4.55	Pass	4.04	Pass
	PG-1C	2.18	0.77	2.85	1.28	3.65	Pass		
18-story	PG-3A	1.91	0.46	4.15	1.32	5.48	Pass	5.54	Pass
	PG-3C	1.78	0.42	4.25	1.32	5.61	Pass		

Note: $\hat{S}_{CT}$ = median collapse intensity; S_{MT} = MCE ground motion spectral demand; CMR = collapse margin ratio; SSF = spectral shape factor; ACMR = adjusted collapse margin ratio; and ACMR_{ave} = average of adjusted collapse margin ratios within performance group.

Table 8. IDA results for subduction earthquakes only

Group	Archetype	$\hat{S}_{CT}$ (g)	S_{MT} (g)	CMR	SSF	ACMR	Pass/fail	$ACMR_{ave}$	Pass/fail
3-story	PG-ThreeStory	2.20	1.50	1.47	1.18	1.73	Pass	1.73	Fail
	PG-ThreeStory2	2.20	1.50	1.47	1.18	1.73	Pass		
8-story	PG-1A	1.26	0.92	1.38	1.25	1.73	Pass	1.68	Fail
	PG-1C	0.98	0.77	1.28	1.28	1.64	Pass		
18-story	PG-3A	0.70	0.46	1.53	1.32	2.02	Pass	2.03	Pass
	PG-3C	0.64	0.42	1.54	1.32	2.03	Pass		

Note: $\hat{S}_{CT}$ = median collapse intensity; S_{MT} = MCE ground motion spectral demand; CMR = collapse margin ratio; SSF = spectral shape factor; ACMR = adjusted collapse margin ratio; and $ACMR_{ave}$ = average of adjusted collapse margin ratios within performance group.

Table 9. IDA results for all earthquakes

Group	Archetype	$\hat{S}_{CT}$ (g)	S_{MT} (g)	CMR	SSF	ACMR	Pass/fail	$ACMR_{ave}$	Pass/fail
3-story	PG-ThreeStory	2.55	1.5	1.70	1.18 (mixed)	2.01 (2.006)	Pass	2.15 (2.046)	Pass
	PG-ThreeStory2	2.9	1.5	1.93	1.18 (mixed)	2.28 (2.086)	Pass		
8-story	PG-1A	1.69	0.92	1.85	1.25 (mixed)	2.31 (2.069)	Pass	2.15 (1.996)	Pass
	PG-1C	1.19	0.77	1.55	1.28 (mixed)	1.98 (1.924)	Pass		
18-story	PG-3A	1.19	0.46	2.58	1.32 (mixed)	3.41 (3.253)	Pass	3.44 (3.28)	Pass
	PG-3C	1.1	0.42	2.62	1.32 (mixed)	3.46 (3.314)	Pass		

Note: $\hat{S}_{CT}$ = median collapse intensity; S_{MT} = MCE ground motion spectral demand; CMR = collapse margin ratio; SSF = spectral shape factor; ACMR = adjusted collapse margin ratio; and $ACMR_{ave}$ = average of adjusted collapse margin ratios within performance group. "Mixed" where SSF = 1.0 for subduction earthquakes.

selected for consideration in Canada was somewhat different from the default 44 ground motions provided by the FEMA P695 procedure. Likewise, consistent with what was observed in Kizilarslan et al. (2021a), the obtained collapse margin ratio values increased for taller buildings. However, for the subduction zone earthquakes, while the individual ACMRS passed the 20% criterion, the average ACMR marginally failed to satisfy the 10% criterion in two of the three groups of archetypes considered. ACMR values of 1.73 and 1.68 were 11.7% and 14.3% lower than the $ACMR_{10\%}$ of 1.96 prescribed by FEMA P695. This showed that, under subduction type earthquakes, slightly more than 10% of the archetypes would collapse. In these cases, 15.8% and 17% actually collapsed. However, the ACMRs were all satisfied globally for the group of 40 earthquakes considered as a whole (Table 9), and that nothing in the methodologies available to date required that results be disaggregated to individually present the results for in-plate/crustal and subduction earthquakes if both were possible at a given geographical location.

Alternatively, it could be logically argued that the spectral shape factor (SSF) for the subduction interface earthquakes should have been 1.0. To take this into account, an additional comparison was done using an SSF value of 1.0 for these earthquakes, and the FEMA P695 SSF values for all the others. As such, ACMRs were calculated for individual earthquakes using the appropriate SSF value, and the resulting mean ACMR value was then obtained. Results using this approach are presented in parenthesis in Table 9 (with SSF values indicated as "mixed"), and again indicated that the structural system met the target value (i.e., "pass").

In spite of the rigor and complexity of the FEMA P695 procedure, the 10% threshold mentioned previously, while being the current consensus of professionals, is arguably a reflection of what is deemed acceptable. As other studies have also found code-compliant structures to have collapse probabilities greatly exceeding 10% when subjected to subduction earthquakes (e.g., Nasser et al. 2019), it is foreseeable that this will be the subject of future discussions. Moreover, it is conceivable that the acceptable probability of collapse under subduction earthquakes could be set to a slightly higher value, and that the results provided here provide a preliminary basis of comparison to fuel such discussions. Finally, additional data showing the failure of archetypes below and above 5% drift are presented in Table 10. Results indicated that failure generally occurred at smaller drifts for subduction zone earthquakes. Notably, because the CC-PSW/CF system was modeled using a strength degradation model taking low-cycle fatigue into account, long duration subduction earthquakes would be expected to introduce a greater reduction in low-cycle fatigue life at a given drift than for non-subduction earthquake.

In spite of the smaller ACMRs obtained for subduction earthquakes, this does not always translate into a noticeable impact on drift demands at the DBE level. Median drift values were 0.89% and 0.83% for the 3-story archetype (PG-ThreeStory), 1.12% and 1.64% for the 8-story archetype (PG-1C), and 0.51% and 1.05% for the 18-story archetypes (PG-3A) for shallow earthquakes and subduction earthquakes, respectively. This showed that, for CC-PSW/CF (for the limited cases considered), DBE drifts for subduction zone earthquakes could be approximately the same or

Table 10. IDA results showing failure conditions

	No. of earthquakes causing failure of archetype			
	Before 5% drift		After 5% drift	
Archetype	Shallow	Subduction	Shallow	Subduction
PG-ThreeStory	0	13	20	7
PG-ThreeStory2	0	13	20	7
PG-1A	4	13	16	7
PG-1C	12	18	8	2
PG-3A	17	18	3	2
PG-3C	16	18	4	2

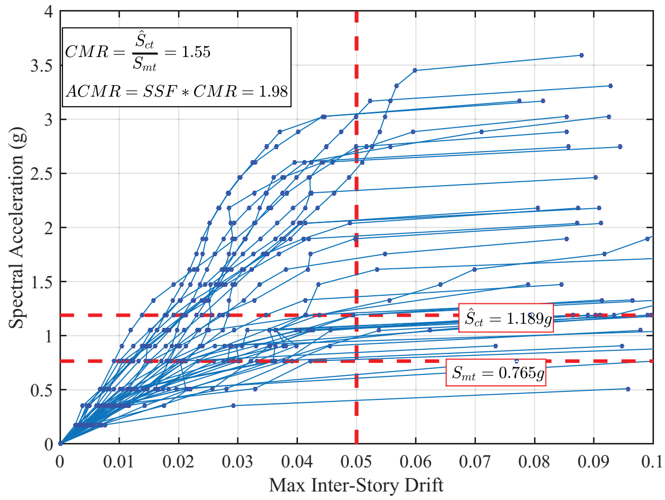

Fig. 3. IDA of PG-1C (with 5% damping anchored at first and fourth periods) for subduction earthquakes only.

up to 45% larger than what is expected in analyses using shallow earthquakes.

Effects of Damping on Disaggregated Results

When considering the above disaggregated data, note that the analysis was conducted using damping values lower than what is rigorously required by FEMA P695. Rayleigh damping coefficients were defined by anchoring the damping values from Eq. (1) at five times the first period and at the fourth period, whereas the procedure actually calls for anchoring at the first and fourth periods. For example, Archetype PG-1C (with the lowest ACMR), considering the extreme anchoring period of five times the first period, resulted in less than 1% damping (instead of 3.3% otherwise) at the first period of vibration for PG-1C, which contributed to more than 80% of the modal participation factor (Bruneau et al. 2019). This was done to prevent overdamping of the structural system when it shifted to higher periods of vibration that ultimately developed near collapse when the composite walls behaved individually after all coupling beams had fractured (those using the FEMA P695 methodology with other structural systems may consider adopting a similar strategy when equally significant period elongations are observed near failure). Consequently, this gives more conservative results.

For comparison, a complementary set of analyses were performed for this archetype using Rayleigh damping anchored between the first period and the fourth period of vibration (consistent with that prescribed by FEMA P695). The resulting ACMR was 1.98, as shown in Fig. 3, which was greater than the required $ACMR_{10\%}$ of 1.96 prescribed by FEMA (meaning that the results in Table 9 now passed instead of marginally failing). However, this would not be the case if instead SSF = 1.0 in Table 8.

Conclusion

This technical note highlighted the difference in collapsed margin ratios obtained with the FEMA P695 methodology for coupled concrete-filled composite plate steel walls using two sets of ground motions. More specifically, the results obtained separately for subduction zone earthquakes and shallow earthquakes were compared. For the latter case, collapse margin ratios were on the same order of magnitude as for those obtained in prior studies on this type of wall. For the subduction zone earthquakes, they were substantially smaller, as expected. While the collapse margin ratios obtained when considering the entire set of earthquakes are still considered satisfactory, this study raised the issue of what should be the acceptable collapse margin ratio for subduction earthquakes alone. This likely will be the subject of future deliberations, and the results obtained here will be informative to fuel discussions.

Data Availability Statement

Some or all data, models, or code that support the findings of this study are available from the corresponding author upon reasonable request.

References

AISC. 2019. "Modern steel construction." Accessed January 20, 2020. https://www.aisc.org/modernsteel/news/2019/august/rainier-square-tower-tops-out-at-850-ft-in-under-10-months/.

AISC. 2021. "SpeedCore." Accessed 15 January, 2023. https://www.aisc.org/why-steel/innovative-systems/SpeedCore/.

AISC. 2022a. *Seismic Provisions for Structural Steel Buildings*. AISC 341. Chicago: AISC.

AISC. 2022b. *Specification for structural steel buildings*. AISC 360. Chicago: AISC.

Bebamzadeh, A., M. Fairhurst, C. Ventura, and J. Sherstobitoff. 2023. "Investigation of the magnitude lower limit on the NBCC2020 seismic hazard." In *Proc., Canadian Conf.—Pacific Conf. on Earthquake Engineering*. Vancouver, BC Canada: CCEE—PCEE.

Broberg, M., S. Shafaei, E. Kizilarslan, J. Seo, A. H. Varma, M. Bruneau, and R. Klemencic. 2022. "Capacity design of coupled composite plate shear wall–concrete-filled system." *J. Struct. Eng.* 148 (4): 04022022. https://doi.org/10.1061/(ASCE)ST.1943-541X.0003296.

Bruneau, M., A. H. Varma, E. Kizilarslan, B. Morgan, S. Shafaei, and J. Seo. 2019. "R-factors for coupled composite plate shear walls/concrete filled (CC-PSW/CF)." Accessed May 15, 2020. https://www.pankowfoundation.org/05-17-r-factors-for-coupled-compositeplate-shear-wallsconcrete-filled-coupled-cpsw/cf.

Bruneau, M., A. H. Varma, S. Shafaei, and D. Huber. 2021. "SpeedCore: Seismic advantages." *Model Steel Constr.* 52–57.

Fazileh, F., R. Fathi-Faz, A. Dolati, C. E. Ventura, M. Saatcioglu, D. Lau, T. Y. Yang, V. Sadeghian, and J. Erochko. 2023. "Methodology for determination of seismic force modification factors in Canada: Performance-based unified procedure." *Earthquake Spectra* 39 (1): 218–241. https://doi.org/10.1177/87552930221144325.

FEMA. 2009. *FEMA P695: Quantification of building seismic performance factors*. Washington, DC: Applied Technology Council. Federal Emergency Management Agency.

Kenarangi, H., E. Kizilarslan, and M. Bruneau. 2020. "Cyclic behavior of c-shaped composite plate shear walls–concrete filled." *Eng. Struct.* 226 (Jan): 111306. https://doi.org/10.1016/j.engstruct.2020.111306.

Kizilarslan, E., M. Broberg, S. Shafaei, A. H. Varma, and M. Bruneau. 2021a. "Seismic design coefficients and factors for coupled composite plate shear walls/concrete filled (CC-PSW/CF)." *Eng. Struct.* 244 (Oct): 112766. https://doi.org/10.1016/j.engstruct.2021.112766.

Kizilarslan, E., M. Broberg, S. Shafaei, A. H. Varma, and M. Bruneau. 2021b. "Non-linear analysis models for composite plate shear walls-concrete filled (C-PSW/CF)." *J. Constr. Steel Res.* 184 (Sep): 106803. https://doi.org/10.1016/j.jcsr.2021.106803.

Kizilarslan, E., and M. Bruneau. 2023. "Cyclic behavior of T-shaped composite plate shear walls concrete filled." *J. Struct. Eng.* 149 (8): 04023102. https://doi.org/10.1061/JSENDH.STENG-11693.

McKenna, F., S. Mazzoni, and G. Fenves. 2016. *Open system for earthquake engineering simulation (OpenSees) software version 2.2. 5*. Berkeley, CA: Univ. of California.

Nasser, A., N. A. Marafi, A. J. Makdisi, M. O. Eberhard, and J. W. Berman. 2019. "Impacts of an M9 Cascadia subduction zone earthquake and Seattle basin on performance of RC core wall buildings." *J. Struct. Eng.* 146 (2): 04019201. https://doi.org/10.1061/(ASCE)ST.1943-541X.0002490.

PEER. 2017. *Guidelines for performance-based seismic design of tall buildings*. PEER Rep. No. 2017/06. Berkeley, CA: Pacific Earthquake Engineering Research Center, Univ. of California.

Shafaei, S., A. H. Varma, J. Seo, and R. Klemencic. 2021. "Cyclic lateral loading behavior of composite plate shear walls/concrete-filled (C-PSW/CF)." *J. Struct. Eng.* 147 (10): 04021145. https://doi.org/10.1061/(ASCE)ST.1943-541X.0003091.

J. Struct. Eng., 2024, 150(8): 06024001